1521-0111/12/8202-143–155$25.00
MOLECULAR PHARMACOLOGY
Vol. 82, No. 2
78097/3780842

Mol Pharmacol 82:143–155, 2012

Localization of a Site of Action for Benzofuroindole-Induced Potentiation of BK_{Ca} Channels[S]

Byoung-Cheol Lee, Hyun-Ho Lim, Songmi Kim, Hyung-Seop Youn, Yuno Lee, Yong-Chul Kim, Soo Hyun Eom, Keun Woo Lee, and Chul-Seung Park

School of Life Sciences (B.-C.L., H.-H.L., H.-S.Y., Y.-C.K., S.H.E., C.-S.P.), National Leading Research Laboratory for Ion Channels (B.-C.L., C.-S.P.), and Cell Dynamic Research Center (B.-C.L., S.H.E., C.-S.P.), Gwangju Institute of Science and Technology, Gwangju, Republic of Korea; Division of Applied Life Science (S.K., Y.L., K.W.L.), Systems and Synthetic Agrobiotech Center (S.K., Y.L., K.W.L.), Plant Molecular Biology and Biotechnology Research Center (S.K., Y.L., K.W.L.), and Research Institute of Natural Science (S.K., Y.L., K.W.L.), Gyeongsang National University, Jinju, Republic of Korea

Received February 3, 2012; accepted April 30, 2012

ABSTRACT

As previously reported, the activity of the large-conductance calcium (Ca^{2+})-activated potassium (K^+) (BK_{Ca}) channel is strongly potentiated from the extracellular side of the cell membrane by certain benzofuroindole derivatives. Here, the mechanism of action of one of the most potent activators, 4-chloro-7-(trifluoromethyl)-10*H*-benzofuro[3,2-*b*]indole-1-carboxylic acid (CTBIC), is characterized. This compound, Compound 22 in the previous report (*Chembiochem* **6:**1745–1748, 2005), potentiated the activity of the channel by shifting its conductance-voltage relationship toward the more negative direction. Cotreatment with CTBIC reduced the affinity of charybdotoxin, a peptide pore-blocker, whereas that of tetraethylammonium, a small pore-blocking quaternary ammonium, was not significantly altered. Guided by these results, scanning mutagenesis of the outer vestibule of the BK_{Ca} channel was launched to uncover the molecular determinants that affect CTBIC binding. Alanine substitution of several amino acid residues in the turret region and the S6 helix of the channel decreased potentiation by CTBIC. Homology modeling and molecular dynamics simulation showed that some of these residues formed a CTBIC binding pocket between two adjacent α-subunits in the outer vestibule of the channel. Thus, it can be envisioned that benzofuroindole derivatives stabilize the open conformation of the channel by binding to the residues clustered across the extracellular part of the subunit interface. The present results indicate that the interface between different α-subunits of the BK_{Ca} channel may play a critical role in the modulation of channel activity. Therefore, this interface represents a potential therapeutic target site for the regulation of K^+ channels.

Introduction

Large-conductance calcium (Ca^{2+})-activated potassium (K^+) channels ($K_{Ca}1.1$ or BK_{Ca}/MaxiK channels) make up a family of K^+-selective ion channels that are activated synergistically by membrane depolarization and an increase in intracellular Ca^{2+} (reviewed in Salkoff et al., 2006; Cui et al., 2009). BK_{Ca} channels are composed of two different subunits: the pore-forming α-subunit and the modulatory β-subunit. Expressed in both excitable and nonexcitable cells, these channels play significant physiological roles in neuronal excitability; action potential repolarization; neurotransmitter and hormone release; tuning of cochlear hair cells; innate immunity; and regulation of tone in vascular, uterine, gastrointestinal, airway, and bladder smooth muscle tissues (Ghatta et al., 2006; Lu et al., 2006). BK_{Ca} channels also perform a central function in the negative feedback control of intracellular Ca^{2+} concentration and thus protect neuronal cells from excess Ca^{2+} influx under pathophysiological conditions (Lawson, 2000). In hyperactive neuronal cells, BK_{Ca} channels restore the membrane potential by down-regulating the activity of voltage-gated sodium (Na^+) and Ca^{2+} chan-

This work was supported in part by the National Leading Research Laboratories [Grant 2011-0028665]; the Cell Dynamics Research Center [Grant 2011-0001154]; and Management of Climate Change Program [Grant 2010-0029084] from National Research Foundation funded by the Ministry of Education, Science and Technology of Korea.

Article, publication date, and citation information can be found at http://molpharm.aspetjournals.org.

http://dx.doi.org/10.1124/mol.112.078097.

[S] The online version of this article (available at http://molpharm.aspetjournals.org) contains supplemental material.

ABBREVIATIONS: BK_{Ca}, large-conductance Ca^{2+}-activated K^+; TBIC, 7-trifluoromethyl-10*H*-benzo[4,5]furo[3,2-*b*]indole-1-carboxylic acid; CTBIC (LDD175), 4-chloro-7-(trifluoromethyl)-10*H*-benzofuro[3,2-*b*]indole-1-carboxylic acid; 3D, three-dimensional; CTX, charybdotoxin; PCR, polymerase chain reaction; DPPC, dipalmitoylphosphatidylcholine; G/G_{max}, relative conductance; *G-V*, conductance-voltage relationship; Slo1, BK_{Ca} channel α-subunit; TEA, tetraethylammonium; P-region, pore region; NS1619, 1,3-dihydro-1-[2-hydroxy-5-(trifluoromethyl)phenyl]-5-(trifluoromethyl)-2*H*-benzimidazol-2-one; BMS 204352, 3-(5-chloro-2-methoxyphenyl)-3-fluoro-1,3-dihydro-6-(trifluoromethyl).

nels (Brenner et al., 2000; Jagger et al., 2000). For these reasons, the potentiation of BK_{Ca} channels may safeguard neuronal cells from damage during or after ischemic stroke. To explore the functional roles of BK_{Ca} channels, researchers have engineered knockout mice that lack these channels. BK_{Ca} channel-deficient mice exhibit incontinence, bladder overactivity, and erectile dysfunction (Meredith et al., 2004; Werner et al., 2005). In addition, a gain-of-function mutant of the BK_{Ca} channel, which imparts enhanced macroscopic channel conductivity, reportedly results in a syndrome whereby generalized human epilepsy and paroxysmal dyskinesia coexist (Du et al., 2005).

BK_{Ca} channels are potential therapeutic targets for several diseases because of their profound involvement in conditions, such as hypertension, coronary artery spasm, urinary incontinence, and a number of neurological disorders (Ghatta et al., 2006). The openers or activators of BK_{Ca} channels can stabilize cells by increasing the efflux of K^+, which leads to hyperpolarization, decrease in cellular excitability, and relaxation of smooth muscle cells. In our previous work, we designed pharmacophores based on the chemical structure of known activators that targeted BK_{Ca} channels. This work resulted in the identification of candidate compounds with appropriately localized functional groups in the benzofuroindole skeleton (Gormemis et al., 2005). We next synthesized several benzofuroindole derivatives and screened them for their channel-opening efficacy by using cloned BK_{Ca} channels expressed in *Xenopus laevis* oocytes. Several of these benzofuroindole derivatives significantly potentiated both the cloned and the native BK_{Ca} channel (Gormemis et al., 2005). Initial characterization of one of the derivatives, TBIC [7-(trifluoromethyl)-10*H*-benzofuro[3,2-*b*]indole-1-carboxylic acid, compound 8], was reported previously (Ha et al., 2006). This compound reversibly activated the BK_{Ca} channel from the extracellular side, and the potentiating effect was not significantly altered by the coexpression of different β-subunits.

In the present study, we investigated the mechanism of action of benzofuroindole compounds on BK_{Ca} channels using a more potent derivative, 4-*c*hloro-7-(trifluoromethyl)-10*H*-benzofuro[3,2-*b*] indole-1-carboxylic acid (CTBIC) (Fig. 1A). CTBIC, initially termed "Compound 22," strongly potentiated the activity of BK_{Ca} channels (Gormemis et al., 2005). This compound (alternatively termed LDD175) significantly reduced bladder voiding frequency and lengthened the intervals between voiding in an animal model by relaxing the bladder smooth muscle (dela Peña et al., 2009). Again, by use of a cloned BK_{Ca} channel expressed in *X. laevis* oocytes, we showed that CTBIC potentiated the channel by shifting its conductance-voltage (G-V) relationship. Furthermore, the binding affinity of charybdotoxin (CTX), a peptide pore-blocker of the BK_{Ca} channel, was decreased in the presence of CTBIC in a concentration-dependent manner. After this observation, an alanine-scanning mutagenesis was performed that targeted the amino acid residues in the outer vestibule of the channel. The functional effects of CTBIC were then investigated using voltage-clamp recording, and the putative binding site of CTBIC was identified using homology modeling and molecular dynamics simulation. Six different residues were identified that significantly affected the affinity of CTBIC; of these, three key residues were clustered in the modeled structure of the BK_{Ca} channel. The current results suggest that the interface formed between the turret region and the loop following the P-region is critical for CTBIC-induced potentiation of the BK_{Ca} channel.

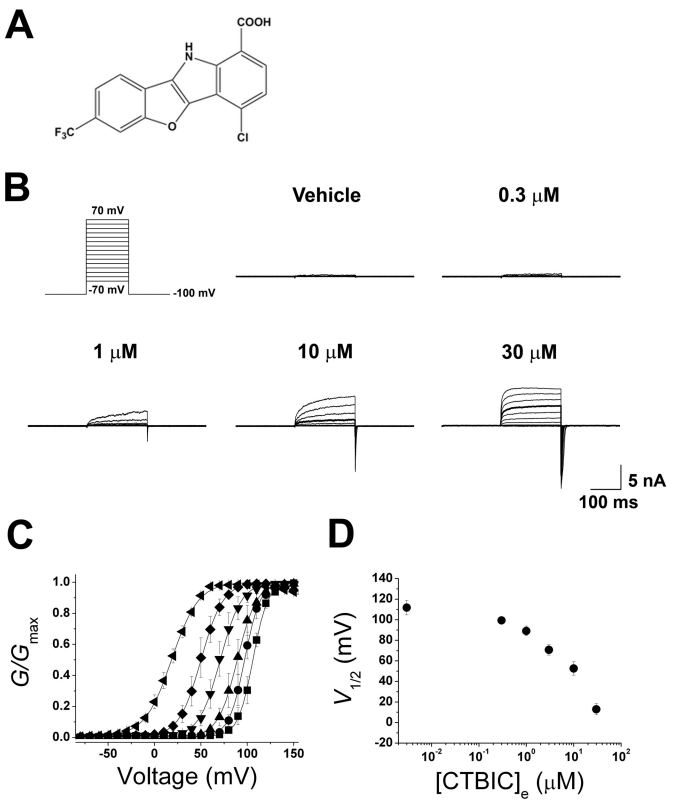

Fig. 1. Strong potentiation of the cloned BK_{Ca} channel by CTBIC. A, structure of CTBIC. B, representative raw traces of macroscopic BK_{Ca} channels in the absence and presence of various concentrations of CTBIC. $[Ca^{2+}]_i$ was fixed at 1 μM, and CTBIC was applied to the extracellular side of the membrane. Ionic currents were evoked with voltage steps of 200 ms to test potentials ranging from −70 to 70 mV in 10-mV increments. The holding voltage was −100 mV. The current traces evoked by a test pulse of 40 mV are highlighted (thick black lines). C, normalized *G-V* relationships of steady-state currents of the BK_{Ca} channel for various concentrations of CTBIC. The symbols represent different concentrations of CTBIC: drug-free (■), 0.3 μM (●), 1 μM (▲), 3 μM (▼), 10 μM (♦), and 30 μM (◀). The membrane was held at a voltage of −100 mV and then stepped from −80 to 150 mV in 10-mV increments. Channel currents were recorded in the presence of 1 μM $[Ca^{2+}]_i$ (n = 11). Conductance values were obtained from peak tail currents and normalized to the maximal conductance observed in the absence of CTBIC. Data points were fitted using the Boltzmann function. D, $V_{1/2}$ of the BK_{Ca} channel at different concentrations of CTBIC. Each data point represents the mean value ± the S.E.M.

Materials and Methods

Reagents. The chemical synthesis of CTBIC was described in a previous study, in which the compound was reported as Compound 22 (Gormemis et al., 2005). CTBIC was dissolved in dimethyl sulfoxide (Sigma-Aldrich, St. Louis, MO) to achieve a 100 mM stock solution. The stock solution was stored at –20°C until use in the patch-clamp experiments, as described below.

Functional Expression of a Cloned BK_{Ca} Channel in *X. laevis* Oocytes. The electrophysiological experiments were performed on *X. laevis* oocytes that expressed the rat BK_{Ca} channel α-subunit (Slo1). The complementary DNAs of the wild-type and mutant channels were subcloned into the pGH oocyte expression vector. The sequence information of the *Slo1* gene used in this study is listed in GenBank under accession number AF135265 (Ha et al., 2000). Each cDNA was subcloned into a pGH expression vector containing the 5′- and 3′-untranslated regions of the *X. laevis* β-glo-

bin gene. These regions have been shown to enhance the expression of certain mammalian messages in *X. laevis* oocytes (Liman et al., 1992). Complementary RNA was prepared in vitro for each construct using T7 RNA polymerase and the mMESSAGE MACHINE (Ambion, Austin, TX). Plasmid DNA was purified and digested with NotI restriction enzyme. RNA was synthesized from linearized plasmid DNA using T7 RNA polymerase in the presence of the cap analog m7G(5′)ppp(5′)G and nucleoside triphosphate.

Oocytes at stages V to VI were surgically removed from the ovarian lobes of anesthetized *X. laevis* (Xenopus I, Dexter, MI) females. The oocytes were transferred into Ca^{2+}-free oocyte Ringer's culture medium (86 mM NaCl, 1.5 mM KCl, 2 mM $MgCl_2$, 10 mM HEPES, and 50 μg/ml gentamicin, pH 7.6). The follicular cell layer was removed by incubating the oocytes in Ca^{2+}-free oocyte Ringer's medium containing 3 mg/ml collagenase (Worthington Biochemicals, Freehold, NJ) for 1 to 2 h. The oocytes were then washed extensively with and kept in ND-96 medium (96 mM NaCl, 2 mM KCl, 1.8 mM $CaCl_2$, 1 mM $MgCl_2$, 5 mM HEPES, and 50 μg/ml gentamicin, pH 7.6). Each oocyte was injected with approximately 50 ng of complementary RNA (in a volume of 50 nl) using a microdispenser (Drummond Scientific, Broomall, PA). Injected oocytes were incubated at 18°C for 1 to 3 days in sterile ND-96 medium. The vitelline membrane was removed manually with fine forceps immediately before the patch-clamp experiments.

Site-Directed Mutagenesis of the BK_{Ca} Channel. Silent mutations initially were introduced to create two unique restriction sites, ClaI (from ATCGAC to ATCGAT) and BssHII (from GCCAGA to GCGCGC) at amino acid positions 152 and 412 of the rat *Slo1* gene, respectively, using two sequential polymerase chain reactions (PCR). Single Ala substitutions (amino acid positions 258–285 and 294–305) were introduced into the outer vestibule of the channel using the cassette mutagenesis methodology. Mutations were generated by PCR using mutagenic primers. The amplified DNA fragments were used to replace the wild-type *Slo1* gene that was cloned into the pGH expression vector using the ClaI and BssHII restriction sites. DNA sequencing was performed to confirm the DNA sequence of each mutant channel using an ABI 377 automatic DNA sequencer (PerkinElmer Life and Analytical Sciences, Waltham, MA).

Electrophysiological Recordings and Data Analysis. All macroscopic current recordings were performed using the gigaohm-seal patch-clamp method in an outside-out configuration. In some experiments, CTBIC or other regents were applied to the extracellular side of the membrane patch to evaluate the impact on the current. All reagents were buffered in a bath solution at pH 7.2 and were applied directly to membrane patches by gravity perfusion using an array of microcapillaries.

Patch pipettes were fabricated from borosilicate glass (WPI, Sarasota, FL) and then fire-polished to a resistance of 5 to 7 MΩ. The channel currents were amplified using an Axopatch 200B amplifier (Molecular Devices, Sunnyvale, CA), low-pass filtered at 1 or 2 kHz using a four-pole Bessel filter, and digitized at a rate of 10 or 20 points/ms using a Digidata 1200A apparatus (Molecular Devices). The ionic currents of expressed channels were activated by voltage-clamp pulses delivered from a holding potential of −100 mV to membrane potentials ranging from −80 to 150 mV in 10-mV increments. The intracellular and extracellular solutions contained the following components, unless otherwise specified: 116 mM KOH, 4 mM KCl, 10 mM HEPES, and 5 mM EGTA, pH 7.2.

To provide the precise free concentration of intracellular Ca^{2+} ($[Ca^{2+}]_i$), the appropriate amount of total Ca^{2+} to be added to the intracellular solution was calculated using MaxChelator software (Patton et al., 2004; http://www.standford.edu/~cpatton/maxc.html). The pH was adjusted to 7.2 with 2-[*N* morpholino]ethanesulfonic acid. To compare the channel characteristics accurately, an identical set of intracellular solutions was used throughout the experiments. Commercial software packages, which included Clampex 8.0 or 8.1 (Molecular Devices) and Origin 6.1 (OriginLab Corp., Northampton, MA), were used for the acquisition and analysis of macroscopic recording data. All data were presented as means ± S.E.M., where *n* indicates the number of independent experiments. For each data set, the significance of the difference was tested using analysis of variance for independent observations. In all cases, $P < 0.05$ was considered significant.

Homology Modeling and Molecular Docking Simulation. The three-dimensional (3D) structure of the BK_{Ca} channel was generated using the homology modeling method. The crystal structure of the mammalian $K_V1.2$ K^+ channel (Protein Data Bank code 2A79) was used as the template. Sequence alignment between the BK_{Ca} channel and the template was carried out using the *Align Sequence to Templates* tool in Discovery Studio (DS) 3.0 (Accelrys, San Diego, CA). The *Build Homology Models* protocol implemented in DS 3.0 was used to build the 3D structure of the BK_{Ca} channel based on the sequence alignment result. The overall stereochemical quality of the final structure was checked with the PROCHECK program (Laskowski et al., 1993). Molecular docking simulations were then performed using the Genetic Optimization for Ligand Docking (GOLD) 4.1 program to predict the binding modes of CTBIC within the modeled BK_{Ca} channel structure. This program uses a genetic algorithm for the docking of flexible ligands into protein binding sites (Jones et al., 1997). The binding site of CTBIC was defined by key amino acid residues considered from experimental data. A radius of 20 Å around the center of the binding site was delineated in the BK_{Ca} channel structure, and genetic algorithm parameters were set as default values. The rotate option was selected for the ring-NHR, ring NR1R1, and protonated carboxylic acids. The best binding mode for CTBIC was obtained using the GoldScore ranking.

Molecular Dynamics Simulation. A molecular dynamics simulation with a dipalmitoylphosphatidylcholine (DPPC) lipid bilayer was carried out using the GROMACS package (version 4.5.3) (Lindahl et al., 2001; Van Der Spoel et al., 2005) to refine the docked CTBIC-BK_{Ca} channel complex. The DPPC model containing 128 DPPC lipids, 3655 water molecules, and GROMACS topologies was downloaded from the website of D.P. Tieleman (http://moose.bio.ucalgary.ca). The GROMOS 53a6 force field (Oosternbrink et al., 2004), including Berger lipid parameters (Berger et al., 1997), was applied. The CTBIC-BK_{Ca} channel complex was embedded in the environment of the 121 DPPC bilayer, which consists of 62 lipids in the upper leaflet and 59 lipids in the lower leaflet. One K^+ ion was placed within the selectivity filter of the structure, and the system was solvated with the simple point charge water model (Berendsen et al., 1981). The membrane system was neutralized by the addition of 11 K^+ counterions. The steepest descent energy minimization was calculated to remove the possible poor contacts from the initial structure until the energy convergence reached 1000 kJ/(mol · nm). The equilibrium simulations were calculated by the constant-temperature, constant-volume ensemble during 100 ps and the isothermal-isobaric ensemble during 1 ns. The temperature of the system was set to 323 K. The normal pressure constant was 1 bar for 1 ns. Heavy atoms and all bonds were constrained by the LINCS algorithm (Ryckaert et al., 1977; Hess et al., 1997). Long range electrostatic interactions were calculated by the particle mesh Ewald method (Darden et al., 1993), and the short-range van der Waals and electrostatic interactions were calculated within a 1.2-nm cutoff. The final production run was carried out for 5 ns under periodic boundary conditions. The integration time step was set to 2 fs, and coordinates were saved for analysis every 2 ps.

Results

Effects of CTBIC on the Macroscopic Currents of Cloned Rat BK_{Ca} Channels Expressed in *X. laevis* Oocytes. In a previous study, we tested a series of benzofuroindole derivatives bearing various functional groups at different positions (Gormemis et al., 2005). CTBIC (or Com-

pound 22) has been the most potent of the compounds tested up until now. This compound contains the following functional groups on the benzofuroindole backbone: a trifluoromethyl group; a carboxyl group; and a chloro group at positions 4, 7, and 1, respectively (Fig. 1A). To characterize the potentiation mechanism of CTBIC, we examined the effect of this compound on the macroscopic currents of a rat BK_{Ca} channel expressed in *X. laevis* oocytes. Both the extracellular (or bath) and intracellular (or pipette) solutions contained symmetrical concentrations of K^+ (120 mM), and the $[Ca^{2+}]_i$ was fixed at 1 μM. Voltage pulses from −70 to 70 mV were applied in 10-mV increments from a holding voltage of −100 mV. The application of CTBIC to the extracellular side of the membrane patch in an outside-out configuration led to the activation of ionic currents at more negative voltages; in addition, the current amplitude at given voltages was greatly increased by CTBIC in a dose-dependent manner (Fig. 1B). The dose-dependent effects of CTBIC can be appreciated by comparing the current traces at 40-mV test pulses at different concentrations of CTBIC (Fig. 1B, thick traces).

The effects of CTBIC on the *G-V* relationships of the BK_{Ca} channel are shown in Fig. 1C. The relative conductance (G/G_{max}) was obtained by normalizing the tail currents (evoked by a step hyperpolarization to −100 mV from a given voltage) to the maximal tail current. The G/G_{max} values at a given concentration of extracellular CTBIC were fitted using a Boltzmann function (Fig. 1C). As the concentration of extracellular CTBIC (i.e., $[CTBIC]_e$) increased, the *G-V* curves progressively shifted toward the negative direction. The shifts in the *G-V* curves were quantified by plotting the half-activation voltage ($V_{1/2}$) against $[CTBIC]_e$ (Fig. 1D). In the absence of CTBIC, the $V_{1/2}$ value was estimated to be 112.7 ± 8.6 mV at 1 μM $[Ca^{2+}]_i$. The progressive increase of $[CTBIC]_e$ shifted the $V_{1/2}$ values nearly 100 mV in the negative direction to an estimated value of 10.6 ± 6.6 mV in the presence of 30 μM CTBIC. Despite the large negative shifts in the position of the *G-V* curve, the slope and the voltage dependence were not significantly altered by external CTBIC, as reported previously for a less potent benzofuroindole derivative, TBIC (Ha et al., 2006).

The N Terminus of the BK_{Ca} Channel Is Not Required for CTBIC-Induced Potentiation. Whereas 10 μM CTBIC potentiated channel currents rapidly and robustly from the extracellular side, the same concentration only marginally affected the channel from the intracellular side for up to 10 s (Supplemental Fig. 1). This result is consistent with our previous observation that TBIC only potentiates the BK_{Ca} channel from the extracellular side (Ha et al., 2006). Because the potentiation of the BK_{Ca} channel by benzofuroindole derivatives was mediated from the extracellular side of the membrane, we investigated whether the N terminus of the BK_{Ca} channel is involved in CTBIC-induced potentiation. The α-subunit of the BK_{Ca} channel (Slo1) contains seven transmembrane domains (S0–S6), and its N terminus is exposed to the extracellular side (Fig. 2A). Earlier work demonstrated that the N-terminal 20 residues of Slo1 were not required for the function of the BK_{Ca} channel (Morrow et al., 2006). Thus, we generated an N-terminal deletion of Slo1 (ΔN20) by using PCR and examined the functional effects on CTBIC potentiation. As shown in Fig. 2B, the current evoked at 120-mV pulse by activation of the ΔN20 channel was significantly increased when CTBIC (30 μM) was applied to the extracellular side of the membrane patch. Furthermore, the *G-V* curve shifted nearly 100 mV in the negative direction under these conditions (Fig. 2C), comparable with the results obtained with the wild-type BK_{Ca} channel (Fig. 1C). These results indicate that the extracellular N terminus of the BK_{Ca} channel is not critical for CTBIC-induced potentiation.

Effects of CTBIC on the Affinity of the Extracellular Channel Blockers Tetraethylammonium and CTX. To obtain mechanistic insights into the CTBIC-induced potentiation of the BK_{Ca} channel, we investigated the effects of CTBIC on two different channel inhibitors: tetraethylammonium (TEA) and CTX. Both TEA, a small quaternary ammonium, and CTX, a 37-amino acid peptide, block ionic currents through the BK_{Ca} channel by occluding the extracellular vestibule (MacKinnon and Miller, 1988; Giangiacomo et al., 1992; Shen et al., 1994).

BK_{Ca} channel currents were inhibited using various concentrations of TEA or CTX in the absence or presence of CTBIC. The effects of CTBIC were first examined on the inhibition of the channel by extracellular TEA. In Fig. 3A, *G-V* relationships are shown for different concentrations of extracellular TEA (0, 0.05, 0.5, and 5 mM). The channel currents were blocked by millimolar concentrations of extracellular TEA, as reported previously (Stanfield, 1983). We then repeated the experiments in the presence of extracellular CTBIC (10 μM) (Fig. 3B). Although the *G-V* curve was shifted by approximately 50 mV in the negative direction by the addition of CTBIC, increasing concentrations of extracellular TEA inhibited the channel current at a similar concentration range. The affinity of TEA for the BK_{Ca} channel was then quantified in the absence and presence of CTBIC (10 and 50 μM). The residual currents (I/I_0) measured at 130 mV were plotted against the extracellular concentration of TEA ($[TEA]_e$), and the data points were fitted using the Hill equation (Fig. 3C). In the absence of CTBIC, channel currents were blocked by extracellular TEA at an apparent dissociation constant (K_d^{app}) of 0.10 ± 0.01 mM, with a Hill coefficient (n_H) of 1.12 ± 0.04 (Fig. 3C, open circles; Supplemental Table 1A). When the membrane patch was cotreated with 50 μM CTBIC, the K_d^{app} value of the TEA blockade was estimated to be 0.11 ± 0.03 mM, virtually identical to the value in the absence of CTBIC. These results indicate that the affinity of TEA was not significantly affected by the binding of CTBIC.

We then examined the effects of CTBIC on the CTX-mediated blockade of the BK_{Ca} channel. In the absence of CTBIC, the channel currents were potently blocked by extracellular CTX in the nanomolar range (Fig. 3D), as reported previously (Anderson et al., 1988). Performance of the same experiment in the presence of CTBIC, however, revealed a significant decrease in the potency of CTX (Fig. 3E). In Fig. 3F, the affinity of CTX in the presence of two different extracellular concentrations of CTBIC ($[CTBIC]_e$) was compared with its affinity in the absence of the drug. In the absence of CTBIC, the K_d^{app} and n_H values of CTX were estimated to be 17.6 ± 2.3 nM and 0.9 ± 0.1, respectively (Supplemental Table 1B). However, the K_d^{app} values increased to 112.3 ± 30.0 and 280.7 ± 19.1 nM in the presence of 10 and 50 μM CTBIC, respectively. Despite the 6.4-fold decrease in CTX affinity in the presence of 10 μM CTBIC, the Hill coefficient was not significantly altered (n_H = 0.7 ± 0.2).

Thus, the extracellular presence of CTBIC significantly

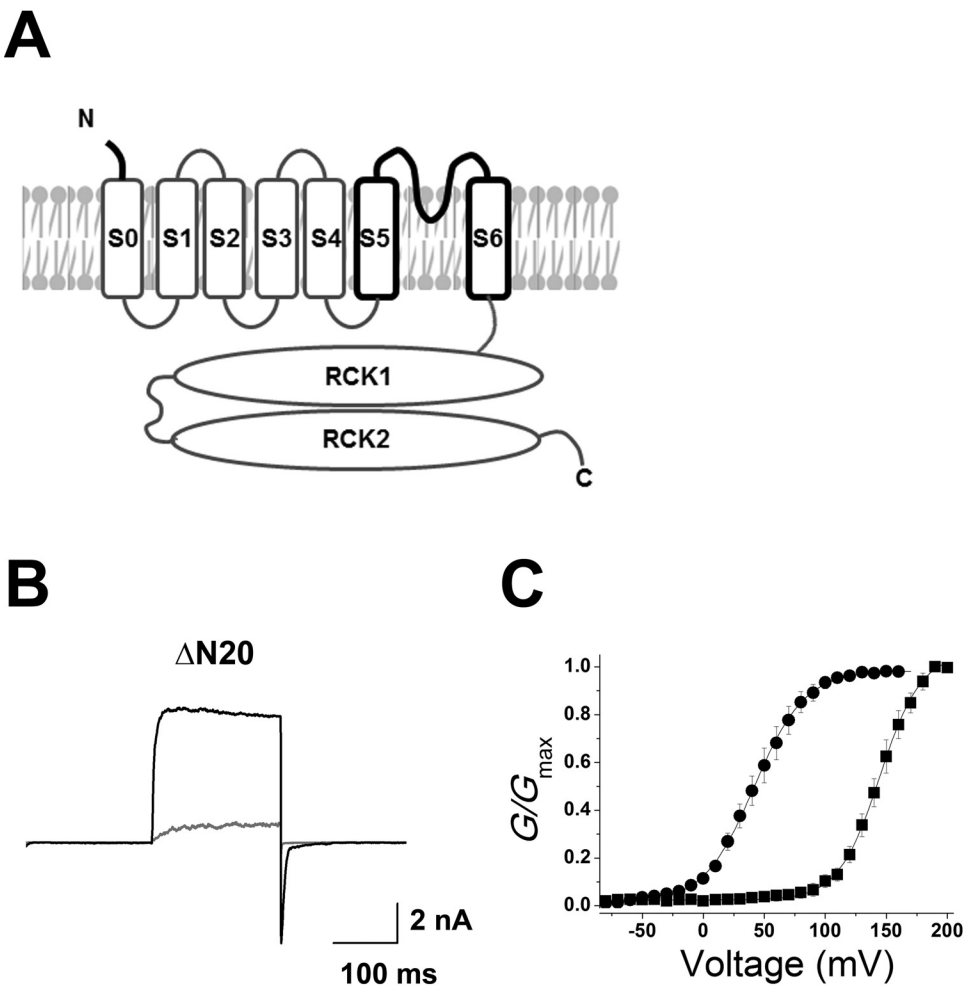

Fig. 2. Effects of N-terminal deletion on CTBIC-induced potentiation. A, membrane topology of the BK_{Ca} channel. The external N terminus is labeled with a bold black line. The outer vestibule of the channel, into which single Ala substitutions were introduced at amino acid positions 258 to 285 and 294 to 305, is also highlighted. The intracellular RCK1 and RCK2 domains, which interact with Ca^{2+} to regulate K^+ conductance, are shown. RCK, regulator of conductance for K^+. B, representative raw traces of the N-terminal deletion mutant (ΔN20). Each line represents the current trace recorded from a 120-mV pulse in the presence of different concentrations of CTBIC: 0 μM (light gray) and 30 μM (black). C, normalized *G-V* relationship of the mutagenized ΔN20 channel. The membrane was held at −100 mV and was then stepped from −80 to 200 mV in 10-mV increments. Channel currents were recorded in the presence of 1 μM $[Ca^{2+}]_i$. The symbols represent different concentrations of CTBIC: 0 μM (■) and 30 μM (●). Data points were fitted using the Boltzmann function.

lowered the affinity of CTX, but not TEA, for the BK_{Ca} channel. Although these findings can be explained in several ways, one intriguing possibility is that the binding site of CTBIC may overlap with the interaction surface (or footprint) of CTX on the BK_{Ca} channel, but not with that of TEA.

Mutational Screening for the Amino Acid Residues that Are Critical for Benzofuroindole-Induced Channel Potentiation. We next attempted to locate the binding site of CTBIC within the BK_{Ca} channel. Guided by the observations that CTBIC potentiated the activity of the BK_{Ca} channel from the extracellular side and that the presence of the compound decreased the affinity of CTX, we focused our attention on the external vestibule of the channel (Figs. 2A and 4A). CTX is known to block several different K^+ channels in a one-to-one stoichiometry by binding to the extracellular loops that flank the K^+-selective pore region (P-region) (MacKinnon, 1991). A series of previous studies revealed a direct interaction between CTX and several amino acid residues on the channel that are involved in the high-affinity binding of the toxin (MacKinnon and Miller, 1989; MacKinnon et al., 1990). Moreover, the structure of the CTX-bacterial K^+ channel KcsA complex is available (Yu et al., 2005) and also illustrates relevant CTX-amino acid interactions. In Fig. 4A, we aligned the amino acid sequence that covers transmembrane domains S5 to S6 of the BK_{Ca} channel with the related sequences in several other K^+ channels. The P-region containing the pore-helix sequence and the selectivity filter, and the two transmembrane domains (S5 and S6, or the homologous outer and inner helices in KcsA) were highly conserved among the K^+ channels. However, poor amino acid sequence conservation was evident in the loop connecting the S5 domain to the P-region (i.e., the "turret" region) and the loop linking the P-region to the S6 domain.

To identify the amino acid residues that affect the affinity of CTBIC, we substituted each residue expected to be exposed on the extracellular side of the membrane (Fig. 4A, black box) with an Ala residue. These residues were contained in the regions of the turret, the pore-helix, the loop in the selectivity filter, and a part of inner helix. As shown in Fig. 4B, most of the residues exposed to extracellular side and located close to the pore region were mutated. On the other hand, we spared the deep pore near the K^+-selectivity filter, because the residues located in this region are known to be essential for the selective permeation of K^+ (Heginbotham et al., 1994).

The wild-type BK_{Ca} channel and 39 different mutant channels harboring a single-point mutation were then expressed in *X. laevis* oocytes, and their functional characteristics were evaluated using electrophysiological recordings. Most of channels were expressed robustly in the oocytes and evoked K^+ currents that were activated by membrane depolarization (data not shown). However, several mutations introduced into the pore-helix (e.g., Y279A, M282A, and T284A) did not result in the expression of functional channels and were

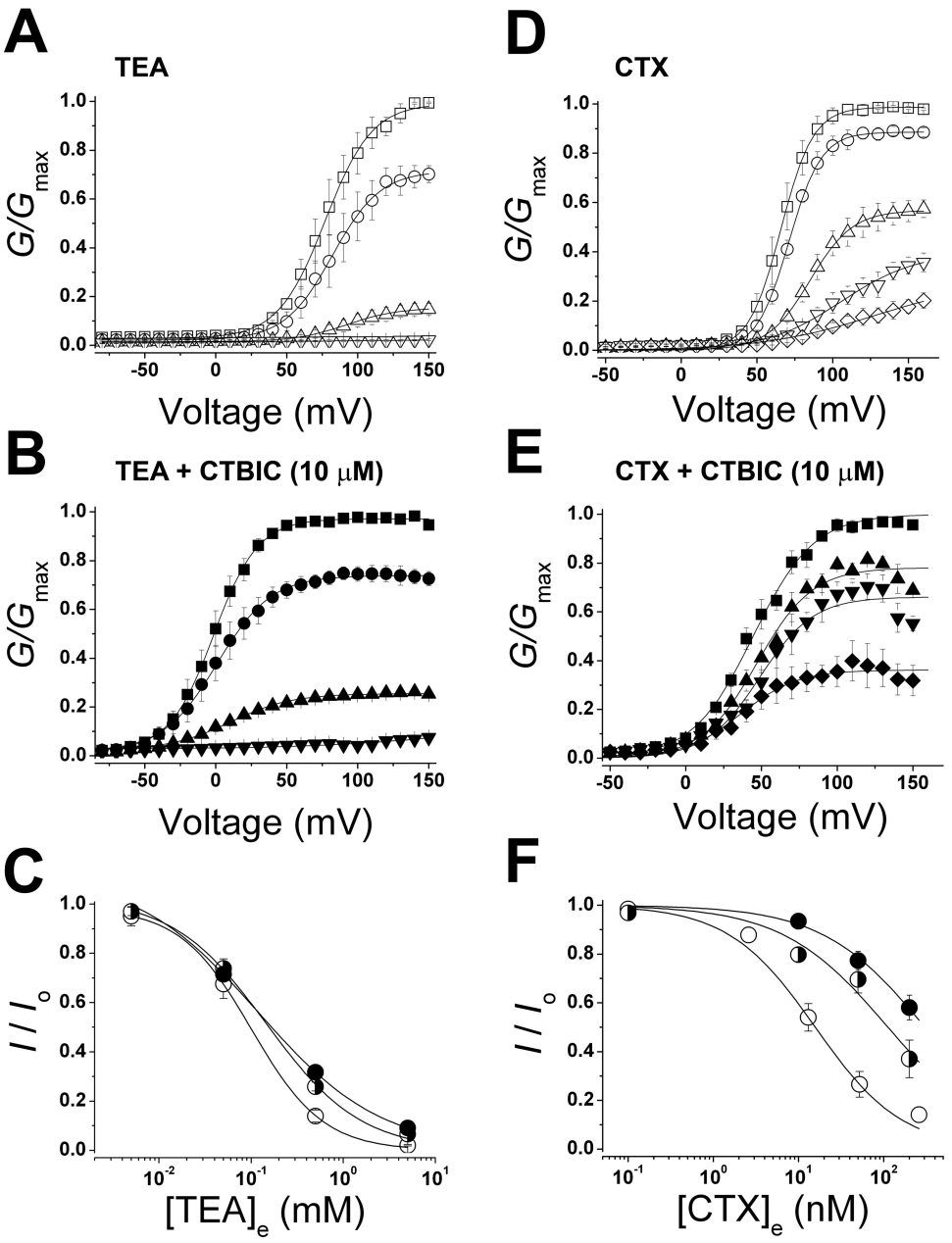

Fig. 3. Effects of CTBIC on the affinity of the two different channel blockers, TEA and CTX. A, normalized *G-V* relationship of the BK_{Ca} channel at various concentrations of TEA in the absence of CTBIC. The symbols represent different concentrations of TEA: 0 μM (□), 0.05 μM (○), 0.5 μM (△), and 5 μM (▽). The membrane was held at −100 mV and was then stepped from −80 to 150 mV in 10-mV increments. Channel currents were recorded in the presence of 1 μM $[Ca^{2+}]_i$ (n = 3). B, normalized *G-V* relationship of the BK_{Ca} channel at various concentrations of TEA in the presence of 10 μM external CTBIC (n = 3). The symbols represent different concentrations of TEA: 0 mM (■), 0.05 mM (●), 0.5 mM (▲), and 5 mM (▼). Data points were fitted using the Boltzmann function. C, inhibition curve of TEA in the absence (○) and presence of CTBIC at 10 μM (◑) and 50 μM (●). The current blockade by TEA is represented as residual currents (I/I_0) obtained from a voltage pulse of 130 mV. Data points were fitted using the Hill function. D, normalized *G-V* relationship of the BK_{Ca} channel at various concentrations of CTX in the absence of CTBIC. The symbols represent different concentrations of CTX: 0 nM (□), 2.6 nM (○), 13 nM (△), 52 nM (▽), and 260 nM (◇). The membrane was held at −100 mV and was then stepped from −80 to 150 mV in 10-mV increments. Currents of the BK_{Ca} channel were recorded in the presence of 1 μM $[Ca^{2+}]_i$ (n = 4). E, normalized *G-V* relationship of the BK_{Ca} channel at various concentrations of CTX in the presence of 10 μM CTBIC (n = 4). The symbols represent different concentrations of CTX: 0 nM (■), 10 (●), 50 nM (▲), and 200 nM (▼). F, inhibition curve of CTX in the absence (○) and presence of CTBIC at 10 μM (◑) and 50 μM (●). Residual currents (I/I_0) were obtained from a voltage pulse of 130 mV.

excluded from the analysis. We also excluded the mutant M285A channel from analysis because this mutation drastically altered the functional characteristics of the channel (data not shown).

The effects of each mutation were then evaluated on the CTBIC-induced potentiation of channel function. Channel currents were recorded in the absence or presence of 30 μM CTBIC at a fixed $[Ca^{2+}]_i$ of 1 μM, and the shifts in the *G-V* curve were monitored. Several mutant channels showed a similar degree of CTBIC-mediated channel activation compared with the wild-type channel. One such example was the P262A mutant, in which the $V_{1/2}$ shift in the presence of 30 μM CTBIC (94.0 ± 2.5 mV) was comparable with that of the wild-type channel (102.1 ± 5.1 mV) (Fig. 4, C and D). However, CTBIC induced a variable degree of channel potentiation in the other mutant channels. For instance, the current potentiation by CTBIC was much weaker for the L299A channels. Thus, the shifts in the *G-V* relationship were correspondingly smaller, yielding a $V_{1/2}$ shift of 72.9 ± 4.7 mV (Fig. 4, C and D).

The effects of Ala substitution on *G-V* curve shifts are summarized in Fig. 5 as the extent of $V_{1/2}$ shifts ($V_{1/2}^{free} - V_{1/2}^{30\ \mu M}$) or the difference in $V_{1/2}$ in the absence of CTBIC ($V_{1/2}^{free}$) and the presence of 30 μM CTBIC ($V_{1/2}^{30\ \mu M}$). The shifts in the $V_{1/2}$ value for most of the mutant channels were similar to that of the wild-type channel; however, nine different mutant channels (D261A, N265A, N268A, T273A, W275A, L299A, R301A, L302A, and M304A) showed significant deviations from the $V_{1/2}$ shift of the wild-type channel. The $V_{1/2}$ shifts of these nine mutant channels were in the range of 73 to 83 mV in the presence of 30 μM CTBIC and were thus decreased by 19 to 29 mV compared with the $V_{1/2}$ shift of the wild-type channel, which can be translated into a 0.44 to 0.67 kcal/mol loss of apparent binding energy (Kim et al., 2006, 2008). Consistent with the results that affinity of TEA was not affected by CTBIC (Fig. 3C),

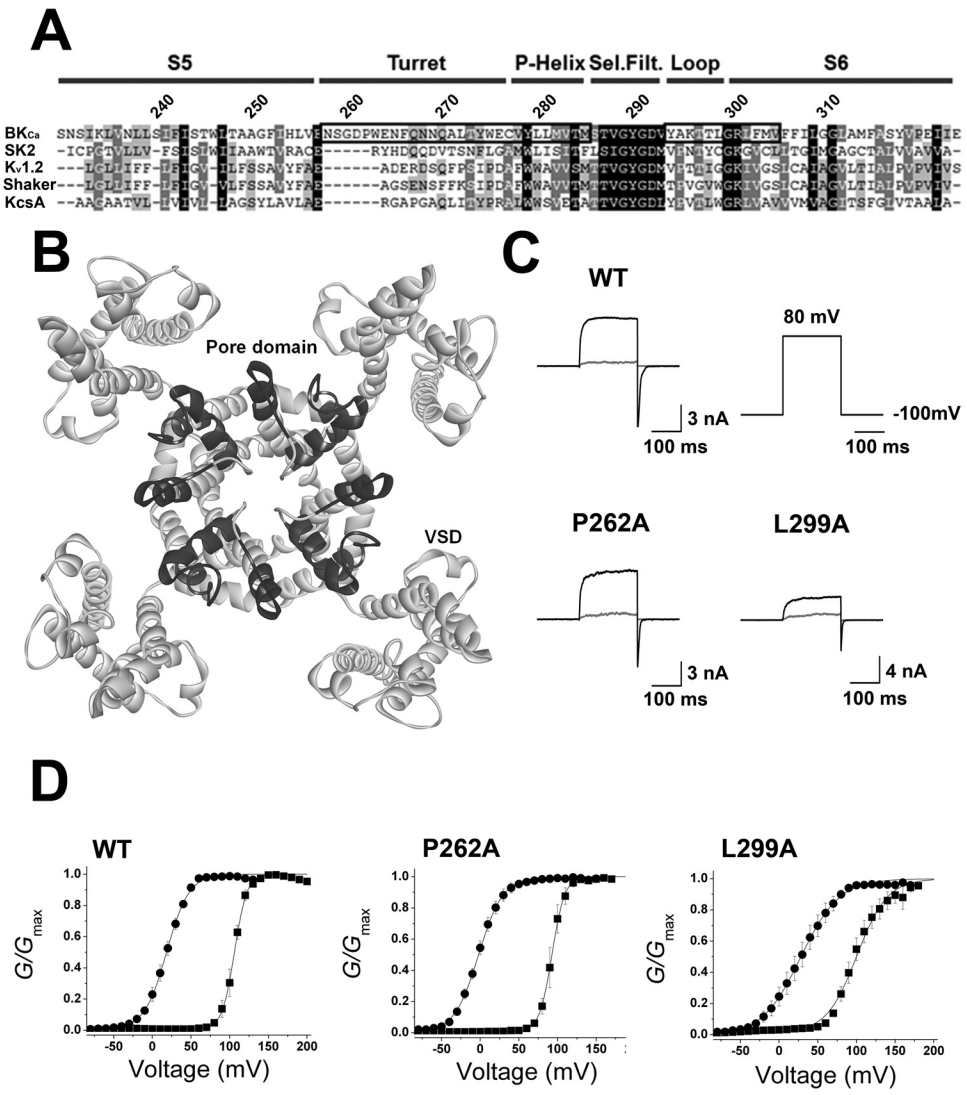

Fig. 4. Ala-scanning mutagenesis at the outer vestibule of the BK_{Ca} channel. A, sequence alignment of amino acids in the vicinity of the pore-forming regions of different K^+ channels. The amino acid sequences of the BK_{Ca}, SK2, $K_v1.2$, Shaker, and KcsA channels were aligned using ClustalX software. The black boxes represent the two regions into which Ala substitutions were introduced. B, homology modeling of the BK_{Ca} channel structure containing the pore domain and the voltage sensor domain. The channel domains, including the S5 domain, the P-region, and the S6 domain, were modeled based on the structure of the $K_V1.2$ channel (Protein Data Bank code 2R9R). Highlighted in black are the two regions in which Ala substitutions were introduced. C, representative raw traces of wild-type, P262A, and L299A mutant channels. Each line represents the current trace recorded from an 80-mV pulse in the presence of different concentrations of CTBIC: 0 μM (light gray) and 30 μM (black). D, normalized *G-V* relationship of wild-type (WT) and mutant channels (P262A and L299A). The membrane was held at −100 mV and was then stepped from −80 to 150 mV in 10-mV increments. Channel currents were recorded in the presence of 1 μM $[Ca^{2+}]_i$. The symbols represent different concentrations of CTBIC: 0 μM (■) and 30 μM (●). Data points were fitted using the Boltzmann function.

the Ala substitution at Tyr294, the extracellular TEA binding site of BK_{Ca} channel (Niu and Magleby, 2002), did not alter $V_{1/2}$ significantly (Fig. 5, Y294A). It is worth pointing out that the $V_{1/2}$ value and the apparent voltage dependence were not significantly different from those of the wild-type channel in the absence of extracellular CTBIC, suggesting that the overall voltage-dependent activation of the channel was not altered significantly by each mutation (Supplemental Fig. 2, A and B). In addition, none of the mutant channels showed increased $V_{1/2}$ shifts with CTBIC treatment, meaning that the potentiation by CTBIC was not augmented by any of the mutations tested.

Association and Dissociation Kinetics of CTBIC Binding to Mutant Channels. We next examined the association and dissociation kinetics of CTBIC in regard to the nine aforementioned mutant channels to localize the binding site for CTBIC more accurately. Because the $V_{1/2}$ shifts induced by CTBIC represent changes in the overall open versus closed equilibrium of the channel because of the binding of the compound, these kinetic data may differentiate between the direct effects of mutation, i.e., loss of direct compound-channel interactions, and the indirect effects of mutation, i.e., CTBIC-induced conformational changes in channel gating.

The time-dependent effects of CTBIC on ionic currents across the membrane patch were monitored every 0.3 s by applying 10-ms step pulses of 100 mV from the holding potential of −100 mV. When 10 μM CTBIC was applied to the extracellular side of the membrane patch, a rapid increase in channel current was observed within 10 s (Fig. 6, time points a and b). After reaching the maximal current level, CTBIC was washed away using the bath solution, and the channel current was observed to decrease over a period of 100 s in the case of the wild-type channel (Fig. 6, time points c and d). Compared with the wild-type channel, the majority of the nine mutant channels showed a similar pattern of current increase with the sudden application of 10 μM CTBIC, as illustrated by the N268A and L302A channels (Fig. 7A, left). In regard to dissociation, however, some of the mutant channels showed a significantly faster decrease in the current trace upon cessation of CTBIC exposure (Fig. 7A, right).

The association and dissociation kinetics of the wild-type and mutant channels were quantified and compared by estimating the time constants of current increase and decrease by fitting the diary plot to a double exponential function. Neither the fast nor the slow component of the association time-constant (τ_{fast} and τ_{slow}) for CTBIC binding was significantly different for the mutant channels compared with the wild-type channel (Supplemental Table 2). However, dissociation time constants for some of the mutant channels were significantly different compared with those of the wild-type

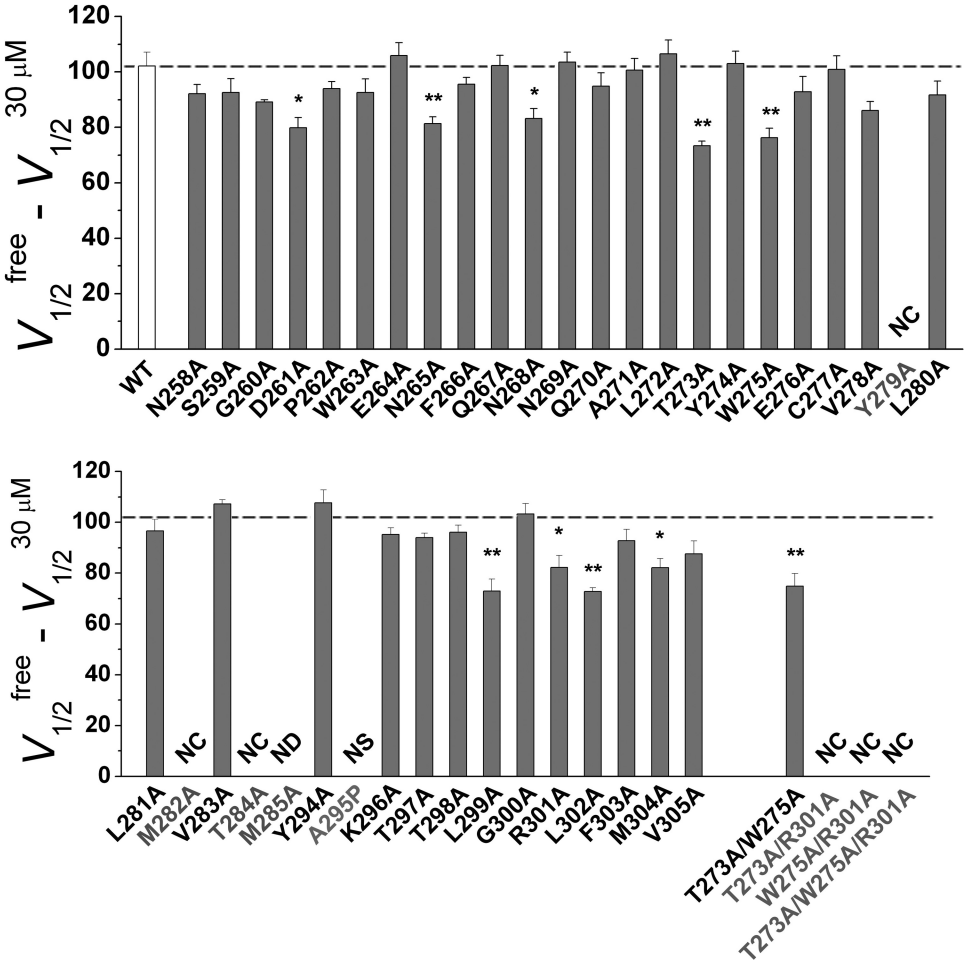

Fig. 5. Differential effects of various point mutations on CTBIC-induced channel potentiation. The effects of point mutations are shown as the difference between $V_{1/2}$ in the absence of CTBIC and the presence of 30 μM CTBIC ($V_{1/2}^{free} - V_{1/2}^{30\ \mu M}$) for the wild-type (empty bar) and 44 different mutant channels (gray bars). The dotted line indicates the mean value of the wild-type channel. Values that significantly differed from the $V_{1/2}$ value of the wild-type channel are indicated (paired Student's t test:*, $P < 0.05$; **, $P < 0.01$). NC, no current; ND, not determined; NS, not studied.

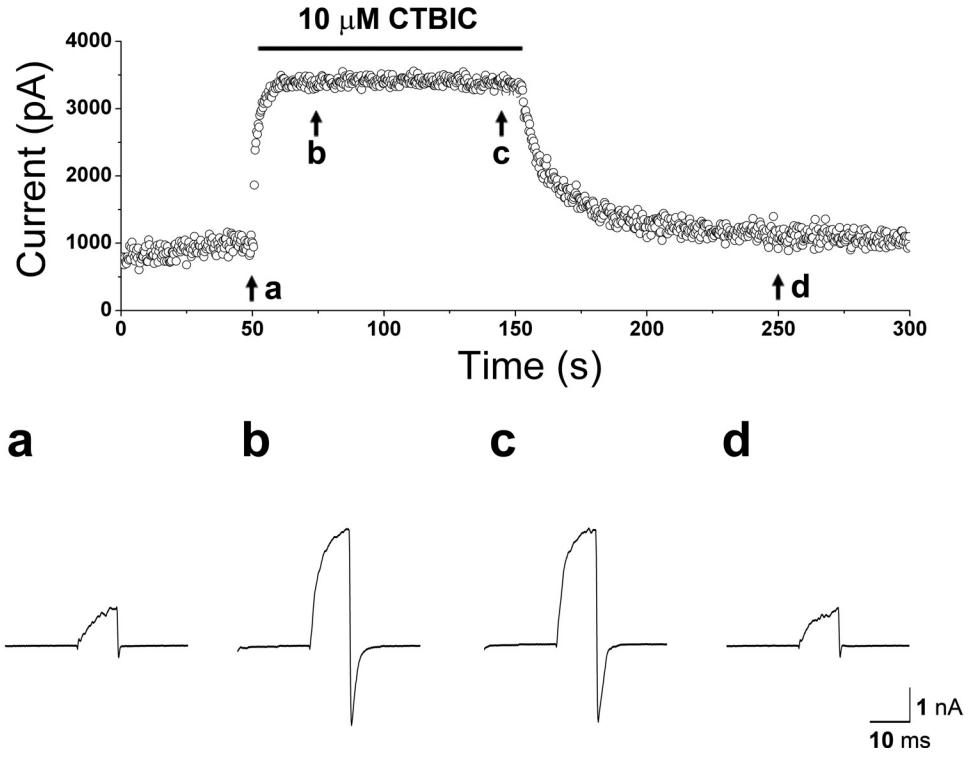

Fig. 6. Reversible activation and deactivation of the BK_{Ca} channel by CTBIC. A diary plot of mean currents evoked by the wild-type BK_{Ca} channel is shown as a continuous recording. The ionic current was elicited every 0.3 s with 10-ms step-pulses of 100 mV from the holding potential of −100 mV. Currents were averaged for 2 ms in between 6 and 8 ms of voltage pulse. Each representative trace (a–d) was obtained at the time indicated by the arrow.

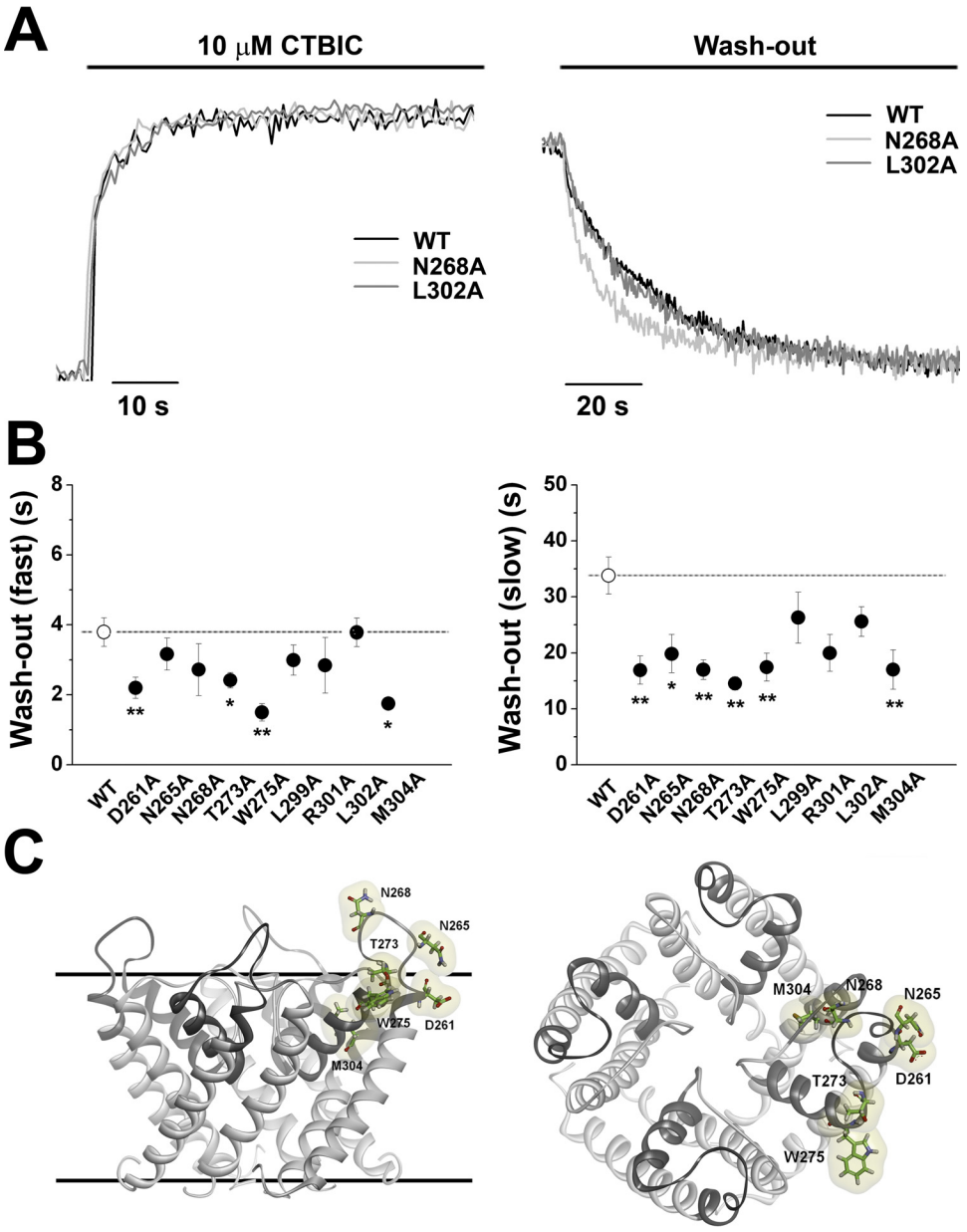

Fig. 7. Association and dissociation kinetics of CTBIC binding to candidate mutant channels. A, representative traces of the association of CTBIC with (left) and the dissociation from (right) the wild-type (black) and mutant channels (N268A, light gray; L302A, dark gray). Each trace was normalized and superimposed with the same time course. B, time constants of CTBIC dissociation. Two different time constants of dissociation, fast (left) and slow (right), were obtained by fitting the traces of the diary plot to a double exponential function. Each data point represents the mean ± S.E.M., and pairs of data points that significantly differed from each other are indicated (paired Student's *t* test:*, $P < 0.05$; **, $P < 0.01$). C, potential binding site of CTBIC mapped within the extracellular vestibule of the BK_{Ca} channel by homology modeling. Side (left) and top (right) views of a structural model for the pore domain of the BK_{Ca} channel (Protein Data Bank code 2A79). Key residues for CTBIC binding are represented by a stick model (green). For simplification, the amino acid residues are visualized in only one of four identical binding sites.

channel (Fig. 7B; Supplemental Table 2). Among the nine candidates, significant decreases were found for four different mutants (D261A, T273A, W275A, and M304A) in the fast component (τ_{fast}) and for six different mutant channels (D261A, N265A, N268A, T273A, W275A, and M304A) in the slow component (τ_{slow}). Because the contribution of the slow component to overall dissociation kinetics is ~0.7, an approximately 2-fold decrease in τ_{slow} affected the dissociation kinetics of CTBIC more significantly (Fig. 7A) than did the decrease in τ_{fast}.

The six mutant channels that demonstrated significant differences in τ_{slow} did so in spite of their similar $\Delta V_{1/2}$ shift values. Therefore, the amino acid residues that were substituted by Ala in these mutant channels that displayed resultantly faster dissociation times can be considered to be candidates for the interaction with CTBIC.

Putative CTBIC Binding Site Revealed in the Interface between the S5 Domain and the Pore-Helix. A modeling study was next carried out using homolog model, molecular docking, and molecular dynamics simulations to predict the binding mode of CTBIC within the BK_{Ca} channel. Sequence alignment was performed with the $K_V1.2$ K^+ channel as the template (Protein Data Bank code 2A79; Long et al., 2005). This channel is a mammalian member of the Shaker-type voltage-gated K^+ channel family and shares approximately 18.0% sequence identity and 41.0% sequence similarity with the BK_{Ca} channel. To validate the modeled structure, the stereochemical quality was evaluated by PROCHECK. The Ramachandran plot obtained by the PROCHECK program showed that 90.0% of residues in the modeled 3D structure resided in the most favored regions and that the overall G-factor was 0.09. Because this model quality is within the range of the average score, our models are reasonable to use for further study. We first mapped the six amino acid residues that were most significantly affected by the mutational electrophysiology studies above on the structure of the modeled BK_{Ca} channel. In the modeled structure, five residues (Asp261, Asn265, Asn268,

Thr273, and Trp275) were clustered within the turret region. The Met304 residue, which is located in the S6-helix (or inner-helix), was also identified in this region (Fig. 7C). It was exciting to find that all six residues reside in the region which CTX can cover (Yu et al., 2005).

To elucidate a potential CTBIC binding site, molecular docking simulation was performed using the validated structure of the BK_{Ca} channel. The CTBIC binding site was defined by the six suggested key amino acid residues (Fig. 7C). The best binding mode was selected based on the consistency of the docked conformations and the fitness score. To refine the docked complex structure, a 5-ns molecular dynamics simulation of the complex was carried out in an explicit membrane environment (i.e., the DPPC lipid bilayer). Refined representative structure (3984-ps frame) was selected from the last 2-ns snapshots. As shown in Fig. 8A, CTBIC was found to interact with the Thr273, Trp275, Glu276, Tyr279, Lys296, and Arg301 residues. The Trp275 residue participated in a π-sigma interaction with the compound, and hydrogen bonding was detected with the Lys296 residue. In particular, three interacting residues (Thr273, Trp275, and Arg301; Fig. 8B) matched residues that were suggested from the experimental studies (Fig. 7B). Thus, the modeling study predicted a reasonable binding mode of CTBIC within the BK_{Ca} channel, providing information about activator-channel interactions at the molecular level.

To validate the putative binding site of CTBIC, we constructed mutant channels in which Thr273, Trp275, and Arg301 were substituted in combination. Two residues were replaced with Ala residues in three different double mutants (T273A/W275A, T273A/R301A, and W275A/R301A), and all three residues were substituted in a triple mutant (T273A/W275A/R301A). Among the four mutants, only one double mutant, T273A/W275A, generated a functional K^+ current (Fig. 5). The $V_{1/2}$ value and the voltage dependence of double mutant channel were not significantly different from those of the wild-type channel (Supplemental Fig. 2, A and B).

Although a single Ala substitution of any of the three residues still produced functional channels, any double or triple mutants containing R301A seemed to become nonfunc-

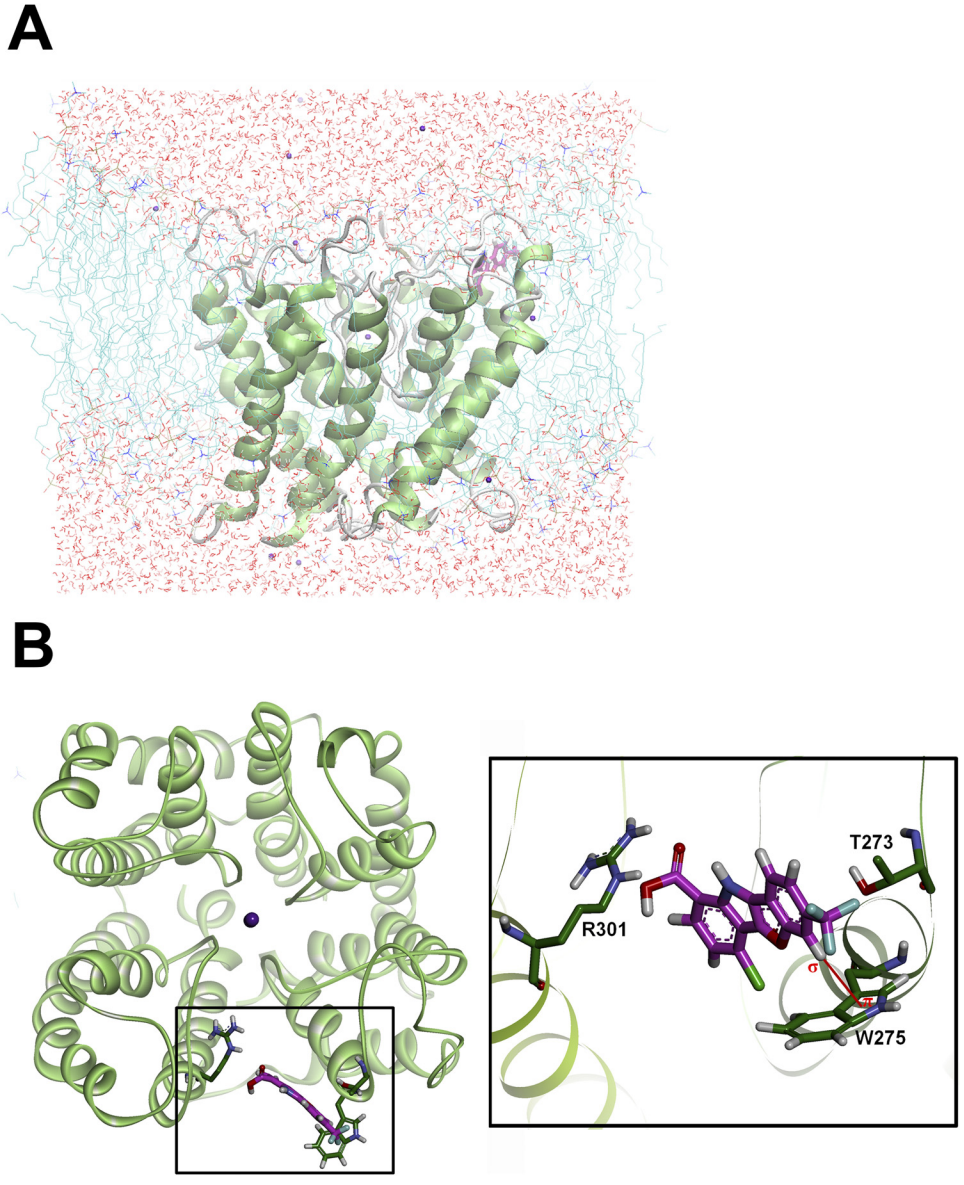

Fig. 8. Binding mode of CTBIC within the BK_{Ca} channel. A, representative structure (3984-ps snapshot) taken from a 5-ns explicit membrane molecular dynamics simulation of CTBIC (magenta stick model) with K^+ ions (violet spheres). The 121 DPPC bilayer and water molecules are displayed by the line model. B, top view of the structure. The detailed binding mode of CTBIC (magenta stick model) with key amino acid residues (green stick model) is highlighted by the black box on the right side of the figure. For simplification, CTBIC binding is visualized in only one of four identical binding sites.

tional. Thus, we investigated the effects of the double mutation, T273A/W275A, on CTBIC-induced potentiation of channel function. Channel currents were recorded in the absence or presence of 30 μM CTBIC, and the shifts in the *G-V* curve were compared with that of wild-type and those of the two single mutant channels. The $V_{1/2}$ shift of T273A/W275A was estimated as 74.9 ± 4.9 mV, which is significantly different from that of the wild-type channel but not much different from those of the two single mutants, which were 73.4 ± 1.7 mV for T273A and 76.3 ± 3.3 mV for W271A, respectively (Fig. 5). Thus, in terms of $V_{1/2}$ shift, the double mutation did not provide any additive or synergistic effects on CTBIC-induced potentiation. We next examined the association and dissociation kinetics of CTBIC with the T273A/W275A double mutant. Contrary to our expectations, the dissociation of CTBIC from the T273A/W275A double mutant was not significantly increased compared with those from the single mutant channels (T273A and W275A) (Fig. 9A). Neither the fast nor the slow component of the dissociation time constant (τ_{fast} and τ_{slow}) for CTBIC binding was significantly different between that of the double mutant channel and those of the single mutant channels (Supplemental Table 2). However, it is intriguing that the association of CTBIC with the T273A/W275A channel was much slower than the associations of the two single mutants (Fig. 9A). Significant increases were found for T273A/W275A in both the fast component (τ_{fast}) and the slow component (τ_{slow}) (Fig. 9B; Supplemental Table 2).

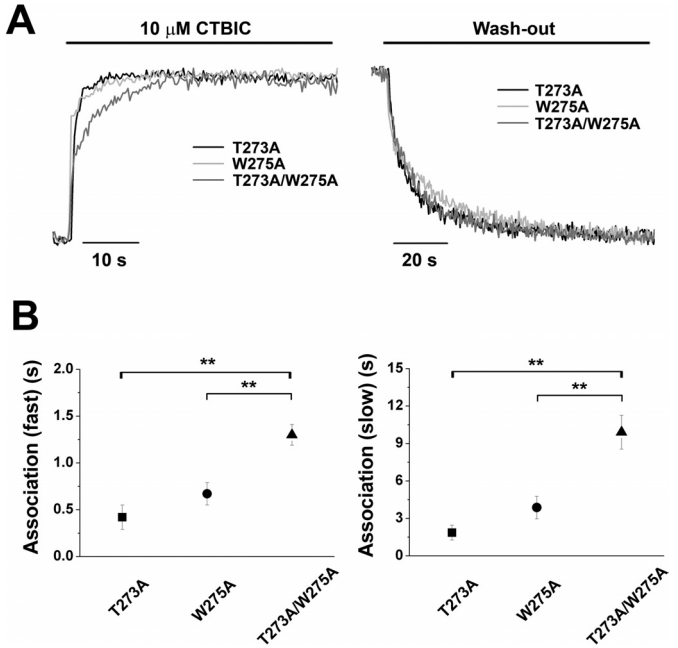

Fig. 9. Effects of a double mutation, T273A and W275A, on CTBIC binding. A, representative traces of the association of CTBIC with (left) and the dissociation from (right) the T273A (black), W275A (light gray), and T273A/W275A (dark gray) mutant channels. Each trace was normalized and superimposed with the same time course. B, time constants of CTBIC association. Two different time constants of association, fast (left) and slow (right), were obtained by fitting the traces of the diary plot to a double exponential function. Each data point represents the mean ± S.E.M., and pairs of data points that significantly differed from each other are indicated (paired Student's *t* test:*, $P < 0.05$; **, $P < 0.01$).

Discussion

The present study investigated the activation mechanism and the potential binding site of a benzofuroindole compound, CTBIC, for the potentiation of the BK_{Ca} channel. We initially observed that the binding affinity of CTX, a pore-blocking peptide toxin, was reduced in the presence of CTBIC in a dose-dependent manner. Guided by these experimental results, we generated a series of Ala-substitution mutations at the loops flanking both sides of the K^+-conduction pore on the extracellular surface of the channel. As part of a scheme to identify the residues that were crucially important for CTBIC-induced channel potentiation, we measured the shifts in *G-V* relationships brought about by extracellular CTBIC under fixed $[Ca^{2+}]_i$ and compared the $V_{1/2}$ values of the wild-type and mutant channels.

By analyzing the effects of the $V_{1/2}$ shifts, we identified nine residues by Ala substitution that significantly decreased the extent of the CTBIC-induced *G-V* shifts. These initial results were somewhat unexpected, and rather surprising, for two reasons. First, the number of amino acid residues affected by Ala substitution seemed to be considerably greater than anticipated. In addition, each residue affected by mutation seemed to contribute to CTBIC binding to a similar, albeit small, extent. Considering the nature of the functional assay used in this study, however, we can only consider these residues as the initial rather than definitive candidates for the binding partners of CTBIC. This is because electrophysiological measurements can only provide the apparent affinity of a ligand, as opposed to an intrinsic binding affinity to its receptor that is afforded by a biochemical binding assay, for example, and the *G-V* curve shift represents the changes in overall equilibrium between a closed and open conformation by the binding of CTBIC.

Thus, it was important to investigate next the association and dissociation kinetics of CTBIC by observing the time-dependent effect of CTBIC on these candidate mutant channels. Assuming that the loss of interaction should increase the dissociation of CTBIC, we were able to narrow down the potential binding residues for CTBIC. Time-dependent plots of both wash-in and wash-out of CTBIC were fitted well with double-exponential functions (Fig. 7A; Supplemental Table 2). We interpret these results as the presence of at least two different time components in both the potentiation and the depotentiation of BK_{Ca} channel by CTBIC, rather than the presence of two different binding sites or binding modes. This idea seems to be supported by the fact that two time-components of both wash-in and wash-out were altered simultaneously by Ala substitutions in several different mutants (Supplemental Table 2). The overall kinetics of CTBIC dissociation seemed to be governed by the slow component (Supplemental Table 2B). Although the association kinetics of CTBIC was not noticeably altered, dissociation was significantly hastened in six of the mutants. Although τ_{slow} values were decreased by only 2-fold in the mutant channels compared with the wild-type channel, the affected mutants showed considerably a faster dissociation of CTBIC because of the larger contribution of the slow component (Fig. 7A).

It was informative as well as intriguing to discover that five of six candidate residues are located in the turret region of the channel. Moreover, the corresponding residues were closely clustered in the 3D structure obtained by homology

modeling of the BK_{Ca} channel (Fig. 7C). Because the turret region is directly connected to the downstream pore-helix sequence and the K^+-selectivity filter, it is conceivable that CTBIC interacts with this region to stabilize the open conformation of the channel.

Our molecular dynamics simulation provided a potential binding mode of CTBIC within the BK_{Ca} channel. CTBIC apparently binds in the interface between two adjacent subunits and interacts with several residues on both subunits. Arg301 on one subunit and Thr273 and Trp275 on the adjacent subunit are especially noteworthy among these residues given the convergence of experimental and modeling results. These three residues were extremely sensitive to combinatorial mutations, and only one double mutant, T273A/W275A, was proven to be functional. It is intriguing to find that the double mutation T273A/W275A significantly affected the association of CTBIC but not its dissociation (Fig. 9A). The association of CTBIC with the double mutant T273A/W275A was much slower than that with the single mutant channels. Thus, the binding affinity of CTBIC for the double mutants should have been dramatically decreased despite that of the similar dissociation kinetics. One plausible interpretation of these results is that the putative binding pocket of CTBIC is significantly altered by the simultaneous removal of the *R*-groups, further supporting the functional importance of the site for CTBIC binding. It may seem inconsistent to find that the double mutant displays no further shift in $V_{1/2}$ value compared with single mutants (Fig. 5), despite the marked reduction in its affinity to CTBIC. However, it is conceivable that the binding energy lost by a certain mutation may not influence the overall equilibrium of channel gating proportionally and, thus, the $V_{1/2}$ value may not be shifted in an additive fashion. It remains to be further confirmed experimentally, however, whether these three amino residues actually interact with CTBIC directly and the binding of this compound CTBIC can provoke local molecular movements, inducing a closed-to-open conformational change of the channel. Given that a series of derivatives of the benzofuroindole skeleton are currently available, a careful combinatorial analysis between mutant channels and diverse compounds may unravel the nature of the interaction and its effects on channel function in future studies.

Many compounds of diverse chemical structures are reported to open the BK_{Ca} channe [e.g., dihydrosoyasaponin-I, maxikidol, NS1619 [1,3-dihydro-1-[2-hydroxy-5-(trifluoromethyl)phenyl]-5-(trifluoromethyl)-2*H*-benzimidazol-2-one], BMS 204352 [3-(5-chloro-2-methoxyphenyl)-3-fluoro-1,3-dihydro-6-(trifluoromethyl)], 17-estradiol, ethylbromide tamoxifen, and epoxyeicosatrienoic acids] (Nardi and Olesen, 2008). Whereas some of these compounds, such as DHS-I and NS1619, were shown to act on the intracellular side of the channel (Holland et al., 1996; Giangiacomo et al., 1998), the binding sites of other activators, including tamoxifen, were located on the extracellular side (Dick et al., 2002). It was also reported that compounds such as BMS-204352 increased the activity of the channel when applied to either the intracellular or the extracellular side of excised membrane patches, although the effects were stronger when the compound was applied to the extracellular side (Gribkoff et al., 2001). However, the specific binding site or site of action of most of these activators has not been investigated in detail. Thus, it will be intriguing to ascertain whether any of the channel activators known to act from the extracellular side of the membrane targets the CTBIC binding site revealed herein and shares a similar mechanism of action. In this regard, it is worth reiterating that the activity of CTBIC is independent of the expression of BK_{Ca} channel β-subunits and does not require the extracellular N terminus of the α-subunit, which is critical for assembly with the β-subunit (Morrow et al., 2006). By contrast, coexpression of specific β-subunits is required for the functional activity of several other BK_{Ca} channel openers, including DHS-I and tamoxifen (Giangiacomo et al., 1998; Dick and Sanders, 2001).

Our results highlight this putative binding site of CTBIC as a potential target for allosteric modulators of additional K^+ channels. Situated at the extracellular border of the plasma membrane, CTBIC interacts with amino acid residues in the turret region and the loop following the P-region. These amino acids are found in each of the four pore-forming α-subunits, at the interface between two α-subunits. Our results are also consistent with the idea that the activation gate of the BK_{Ca} channel may reside within the selectivity filter rather than within the cytoplasmic region (Li and Aldrich, 2006; Piskorowski and Aldrich, 2006; Tang et al., 2009; Thompson and Begenisich, 2012). Because of the proximity and the continuity to the pore-helix, the interaction of CTBIC with its binding pocket may influence the activation gating of the BK_{Ca} channel, which occurs at the K^+-selective pore itself. In addition, the putative binding site of CTBIC revealed in this study coincides with the footprint of a bivalent tarantula toxin of the TRPV1 channel (Bohlen et al., 2010). This dimeric peptide activates TRPV1 channels by binding to the extracellular region of the channel pore. These results further support the significance of extracellular pore region for conformational changes during channel activation. The turret region and the loop are not only accessible from the extracellular side of the membrane but are also highly diverse in their amino acid sequences among different subclasses of K^+ channels. In light of the fact that exquisite specificity has been one of the most challenging tasks in the development of drugs that can regulate voltage-gated ion channels, these amino acid sequences can potentially be targeted to obtain subtype-specific modulators of K^+ channels.

In conclusion, we localized the potential binding site of the benzofuroindole CTBIC within the BK_{Ca} channel and postulated a mechanism of action for its augmentation of channel potentiation. Our present results emphasize the extracellular interface between two α-subunits as a potential target for allosteric modulation of the BK_{Ca} channel and for the development of drugs that interact with K^+ channels, in general.

Acknowledgments

We are grateful to the members of the Laboratory of Molecular Neurobiology at GIST for their valuable comments and timely help throughout the work. We thank Dr. C. Miller at Brandeis University for providing the recombinant CTX.

Authorship Contributions

Participated in research design: B.-C. Lee, Lim, and Park.
Conducted experiments: B.-C. Lee, Lim, S. Kim, and Youn.
Contributed new reagents or analytic tools: Y.-C. Kim, Y. Lee, K.W. Lee, and Eom.
Performed data analysis: B.-C. Lee, Lim, and S. Kim.
Wrote or contributed to the writing of the manuscript: B.-C. Lee, S. Kim, and Park.

References

Anderson CS, MacKinnon R, Smith C, and Miller C (1988) Charybdotoxin block of single Ca^{2+}-activated K^+ channels. Effects of channel gating, voltage, and ionic strength. *J Gen Physiol* **91:**317–333.

Berger O, Edholm O, and Jähnig F (1997) Molecular dynamics simulations of a fluid bilayer of dipalmitoylphosphatidylcholine at full hydration, constant pressure, and constant temperature. *Biophys J* **72:**2002–2013.

Berendsen H, Postma J, Van Gunsteren W and Hermans J (1981) Interaction models for water in relation to protein hydration. In: *Intermolecular Forces: Proceedings of the Fourteenth Jerusalem Symposium in Quantum Chemistry and Biochemistry* (Pullman B ed) pp. 331–342, D. Reidel Publishing Co., Dordrecht, Holland.

Bohlen CJ, Priel A, Zhou S, King D, Siemens J, and Julius D (2010) A bivalent tarantula toxin activates the capsaicin receptor, TRPV1, by targeting the outer pore domain. *Cell* **141:**834–845.

Brenner R, Peréz GJ, Bonev AD, Eckman DM, Kosek JC, Wiler SW, Patterson AJ, Nelson MT, and Aldrich RW(2000) Vasoregulation by the beta1 subunit of the calcium-activated potassium channel. *Nature* **407:**870–876.

Cui J, Yang H, and Lee US (2009) Molecular mechanisms of BK channel activation. *Cell Mol Life Sci* **66:**852–875.

Darden T, York D, and Pedersen L (1993) Particle mesh Ewald: An N log (N) method for Ewald sums in large systems. *J Chem Phys* **98:**10089–10092.

dela Peña IC, Yoon SY, Kim SM, Lee GS, Ryu JH, Park CS, Kim YC, and Cheong JH (2009) Bladder-relaxant properties of the novel benzofuroindole analogue LDD175. *Pharmacology* **83:**367–378.

Dick GM, Hunter AC, and Sanders KM (2002) Ethylbromide tamoxifen, a membrane-impermeant antiestrogen, activates smooth muscle calcium-activated large-conductance potassium channels from the extracellular side. *Mol Pharmacol* **61:** 1105–1113.

Dick GM and Sanders KM (2001) (Xeno)estrogen sensitivity of smooth muscle BK channels conferred by the regulatory beta1 subunit: a study of beta1 knockout mice. *J Biol Chem* **276:**44835–44840.

Du W, Bautista JF, Yang H, Diez-Sampedro A, You SA, Wang L, Kotagal P, Lüders HO, Shi J, Cui J, et al. (2005) Calcium-sensitive potassium channelopathy in human epilepsy and paroxysmal movement disorder. *Nat Genet* **37:**733–738.

Ghatta S, Nimmagadda D, Xu X, and O'Rourke ST (2006) Large-conductance, calcium-activated potassium channels: structural and functional implications. *Pharmacol Ther* **110:**103–116.

Giangiacomo KM, Garcia ML, and McManus OB (1992) Mechanism of iberiotoxin block of the large-conductance calcium-activated potassium channel from bovine aortic smooth muscle. *Biochemistry* **31:**6719–6727.

Giangiacomo KM, Kamassah A, Harris G, and McManus OB (1998) Mechanism of maxi-K channel activation by dehydrosoyasaponin-I. *J Gen Physiol* **112:**485–501.

Gormemis AE, Ha TS, Im I, Jung KY, Lee JY, Park CS, and Kim YC (2005) Benzofuroindole analogues as potent BK(Ca) channel openers. *Chembiochem* **6:**1745–1748.

Gribkoff VK, Starrett JE Jr, Dworetzky SI, Hewawasam P, Boissard CG, Cook DA, Frantz SW, Heman K, Hibbard JR, Huston K, et al. (2001) Targeting acute ischemic stroke with a calcium-sensitive opener of maxi-K potassium channels. *Nat Med* **7:**471–477.

Ha TS, Jeong SY, Cho SW, Jeon H, Roh GS, Choi WS, and Park CS (2000) Functional characteristics of two BK_{Ca} channel variants differentially expressed in rat brain tissues. *Eur J Biochem* **267:**910–918.

Ha TS, Lim HH, Lee GE, Kim YC, and Park CS (2006) Electrophysiological characterization of benzofuroindole-induced potentiation of large-conductance Ca^{2+}-activated K^+ channels. *Mol Pharmacol* **69:**1007–1014.

Heginbotham L, Lu Z, Abramson T, and MacKinnon R (1994) Mutations in the K^+ channel signature sequence. *Biophys J* **66:**1061–1067.

Hess B, Bekker H, Berendsen HJ, and Fraaije JG (1997) LINCS: a linear constraint solver for molecular simulations. *J Comput Chem* **18:**1463–1472.

Holland M, Langton PD, Standen NB, and Boyle JP (1996) Effects of the BK_{Ca} channel activator, NS1619, on rat cerebral artery smooth muscle. *Br J Pharmacol* **117:**119–129.

Jagger DJ, Griesinger CB, Rivolta MN, Holley MC, and Ashmore JF (2000) Calcium signalling mediated by the 9 acetylcholine receptor in a cochlear cell line from the immortomouse. *J Physiol* **527:**49–54.

Jones G, Willett P, Glen RC, Leach AR, and Taylor R (1997) Development and validation of a genetic algorithm for flexible docking. *J Mol Biol* **267:**727–748.

Kim HJ, Lim HH, Rho SH, Bao L, Lee JH, Cox DH, Kim do H, and Park CS (2008) Modulation of the conductance-voltage relationship of the BK Ca channel by mutations at the putative flexible interface between two RCK domains. *Biophys J* **94:**446–456.

Kim HJ, Lim HH, Rho SH, Eom SH, and Park CS (2006) Hydrophobic interface between two regulators of K^+ conductance domains critical for calcium-dependent activation of large conductance Ca^{2+}-activated K^+ channels. *J Biol Chem* **281:** 38573–38581.

Laskowski RA, Moss DS, and Thornton JM (1993) Main-chain bond lengths and bond angles in protein structures. *J Mol Biol* **231:**1049–1067.

Lawson K (2000) Is there a role for potassium channel openers in neuronal ion channel disorders? *Expert Opin Investig Drugs* **9:**2269–2280.

Li W and Aldrich RW (2006) State-dependent block of BK channels by synthesized shaker ball peptides. *J Gen Physiol* **128:**423–441.

Liman ER, Tytgat J, and Hess P (1992) Subunit stoichiometry of a mammalian K^+ channel determined by construction of multimeric cDNAs. *Neuron* **9:**861–871.

Lindahl E, Hess B, and Van Der Spoel D (2001) GROMACS 3.0: a package for molecular simulation and trajectory analysis. *J Mol Model* **7:**306–317.

Long SB, Campbell EB, and Mackinnon R (2005) Crystal structure of a mammalian voltage-dependent Shaker family K^+ channel. *Science* **309:**897–903.

Lu R, Alioua A, Kumar Y, Eghbali M, Stefani E, and Toro L (2006) MaxiK channel partners: physiological impact. *J Physiol* **570:**65–72.

MacKinnon R(1991) Determination of the subunit stoichiometry of a voltage-activated potassium channel. *Nature* **350:**232–235.

MacKinnon R, Heginbotham L, and Abramson T (1990) Mapping the receptor site for charybdotoxin, a pore-blocking potassium channel inhibitor. *Neuron* **5:**767–771.

MacKinnon R and Miller C (1988) Mechanism of charybdotoxin block of the high-conductance, Ca^{2+}-activated K^+ channel. *J Gen Physiol* **91:**335–349.

MacKinnon R and Miller C (1989) Mutant potassium channels with altered binding of charybdotoxin, a pore-blocking peptide inhibitor. *Science* **245:**1382–1385.

Meredith AL, Thorneloe KS, Werner ME, Nelson MT, and Aldrich RW (2004) Overactive bladder and incontinence in the absence of the BK large conductance Ca^{2+}-activated K^+ channel. *J Biol Chem* **279:**36746–36752.

Morrow JP, Zakharov SI, Liu G, Yang L, Sok AJ, and Marx SO (2006) Defining the BK channel domains required for beta1-subunit modulation. *Proc Natl Acad Sci USA* **103:**5096–5101.

Nardi A and Olesen SP (2008) BK channel modulators: a comprehensive overview. *Curr Med Chem* **15:**1126–1146.

Niu X and Magleby KL (2002) Stepwise contribution of each subunit to the cooperative activation of BK channels by Ca^{2+}. *Proc Natl Acad Sci USA* **99:**11441–11446.

Oostenbrink C, Villa A, Mark AE, and van Gunsteren WF (2004) A biomolecular force field based on the free enthalpy of hydration and solvation: the GROMOS force-field parameter sets 53A5 and 53A6. *J Comput Chem* **25:**1656–1676.

Patton C, Thompson S, and Epel D (2004) Some precautions in using chelators to buffer metals in biological solutions. *Cell Calcium* **35:**427–431.

Piskorowski RA and Aldrich RW (2006) Relationship between pore occupancy and gating in BK potassium channels. *J Gen Physiol* **127:**557–576.

Ryckaert JP, Ciccotti G, and Berendsen HJ (1977) Numerical integration of the cartesian equations of motion of a system with constraints: molecular dynamics of n-Alkanes. *J Comput Phys* **23:**327–341.

Salkoff L, Butler A, Ferreira G, Santi C, and Wei A (2006) High-conductance potassium channels of the SLO family. *Nat Rev Neurosci* **7:**921–931.

Shen KZ, Lagrutta A, Davies NW, Standen NB, Adelman JP, and North RA (1994) Tetraethylammonium block of Slowpoke calcium-activated potassium channels expressed in Xenopus oocytes: evidence for tetrameric channel formation. *Pflugers Arch* **426:**440–445.

Stanfield PR (1983) Tetraethylammonium ions and the potassium permeability of excitable cells. *Rev Physiol Biochem Pharmacol* **97:**1–67.

Tang QY, Zeng XH, and Lingle CJ (2009) Closed-channel block of BK potassium channels by bbTBA requires partial activation. *J Gen Physiol* **134:**409–436.

Thompson J and Begenisich T (2012) Selectivity filter gating in large-conductance Ca^{2+}-activated K^+ channels. *J Gen Physiol* **139:**235–244.

Van Der Spoel D, Lindahl E, Hess B, Groenhof G, Mark AE, and Berendsen HJ (2005) GROMACS: fast, flexible, and free. *J Comput Chem* **26:**1701–1718.

Werner ME, Zvara P, Meredith AL, Aldrich RW, and Nelson MT (2005) Erectile dysfunction in mice lacking the large-conductance calcium-activated potassium (BK) channel. *J Physiol* **567:**545–556.

Yu L, Sun C, Song D, Shen J, Xu N, Gunasekera A, Hajduk PJ, and Olejniczak ET (2005) Nuclear magnetic resonance structural studies of a potassium channel-charybdotoxin complex. *Biochemistry* **44:**15834–15841.

Address correspondence to: Dr. Chul-Seung Park, School of Life Sciences, Gwangju Institute of Science and Technology (GIST), 123 Cheomdangwagi-ro, Buk-gu, Gwangju, 500-712, Korea. E-mail: cspark@gist.ac.kr